crystals

MDPI

Article

Ultra-High-Speed Growth of GaAs Solar Cells by Triple-Chamber Hydride Vapor Phase Epitaxy

Ryuji Oshima [1,*], Akio Ogura [2], Yasushi Shoji [1], Kikuo Makita [1], Akinori Ubukata [3], Shuuichi Koseki [3], Mitsuru Imaizumi [2] and Takeyoshi Sugaya [1]

[1] Global Zero Emission Research Center, National Institute of Advanced Industrial Science and Technology, Tsukuba 305-8568, Ibaraki, Japan
[2] Japan Aerospace Exploration Agency, Tsukuba 305-8505, Ibaraki, Japan
[3] Taiyo Nippon Sanso Corporation, Tsukuba 300-2611, Ibaraki, Japan
* Correspondence: r.oshima@aist.go.jp

Abstract: In photovoltaic (PV) power generation, highly efficient III-V solar cells are promising for emerging mobile applications, such as vehicle-integrated PVs. Although hydride vapor phase epitaxy (HVPE) has received attention due to its lower fabrication costs, realization of high throughput performance while maintaining solar-cell characteristics using this growth method is essential. In this study, the effect of atmospheric-pressure triple-chamber HVPE growth conditions on GaAs solar-cell properties were carefully investigated in conjunction with defect analysis using deep-level transient spectroscopy (DLTS). Based on the analysis on GaAs reaction processes, the suppression of arsine thermal cracking in the HVPE hot-wall reactor was important to achieve fast GaAs growth using a low input V/III ratio. Moreover, the DLTS results revealed that the reduced input V/III ratio was effective in suppressing the generation of EL2 traps, which is a common GaAs midgap complex defect involving arsenic antisites. Although the EL2 trap density increased with the growth rate, the performance of GaAs solar cells that were grown under reduced arsine thermal cracking exhibited almost no considerable cell parameter deterioration at a growth rate of up to 297 μm/h. Consequently, a conversion efficiency of 24% with a high open-circuit voltage of 1.04 V was achieved for the cells that were grown at 200 μm/h.

Keywords: III-V semiconductors; hydride vapor phase epitaxy; solar cells; deep-level transient spectroscopy

Citation: Oshima, R.; Ogura, A.; Shoji, Y.; Makita, K.; Ubukata, A.; Koseki, S.; Imaizumi, M.; Sugaya, T. Ultra-High-Speed Growth of GaAs Solar Cells by Triple-Chamber Hydride Vapor Phase Epitaxy. *Crystals* **2023**, *13*, 370. https://doi.org/10.3390/cryst13030370

Academic Editors: Stephanie Tomasulo and Aaron Ptak

Received: 1 February 2023
Revised: 14 February 2023
Accepted: 18 February 2023
Published: 21 February 2023

1. Introduction

The importance of renewable energy has increased with increased realization of a decarbonized society. This is particularly true for photovoltaic (PV) power generation, which has garnered increasing interest in terms of mobile applications, such as unmanned aircraft and vehicle-integrated PVs, in addition to conventional applications that are already in use today [1]. As this emerging usage of renewable energy-powered devices has a limited environmental footprint but requires high power generation, highly efficient III-V solar cells, which are currently used in space and concentrating PV applications, are promising for such applications. However, one obstacle for implementing such solar cells is their current high manufacturing cost. Recently, research on lowering the cost of III-V solar cells has been conducted that includes low-cost growth method development and substrate reuse. Regarding substrate reuse, delamination of devices via epitaxial liftoff [2] or controlled spalling techniques [3] are promising candidates. Moreover, these techniques can be extended to heterogeneous tandem solar cells through wafer bonding. For example, two- or four-terminal III-V/Si triple-junctions with conversion efficiency (η) = 35.9% and two-terminal III-V/Cu–In–Ga–Se (CIGS) triple-junctions with η = 29.3% have been successfully demonstrated [4–7].

In terms of the growth method, reducing fabrication costs while maintaining solar-cell performance is essential for developing the aforementioned applications. Hydride vapor phase epitaxy (HVPE) can enable the replacement of expensive group-III metalorganic precursors used in metalorganic vapor phase epitaxy (MOVPE) with cheaper metal chlorides while achieving fast growth rates of several-hundred microns per hour [8,9]. Increased throughput performance will considerably reduce the depreciation cost of growth tools because more wafers can be produced using a single tool over its lifetime, which is crucial for mass production. Therefore, we have developed atmospheric-pressure triple-chamber HVPE systems for fabricating solar cell structures. So far, we have demonstrated GaAs solar cells with η = 22.1% and GaInP solar cells with η = 15.4% by improving their heterointerface quality [10,11]. Moreover, we have presented GaInP/GaAs dual-junction (2J) solar cells with η = 28.3% grown with AlGaInP passivation layers using aluminum trichloride ($AlCl_3$) as the group-III precursor [12]. The growth rates for *p*-GaAs and *p*-GaInP base layers were 24 and 38 µm/h, respectively. Boyers also presented 2J solar cells with η = 28.0% at a growth rate of 60 µm/h for both materials using a dynamic HVPE system [13]. Thus, in terms of proof-of-concept for mass production, higher-quality 2J solar cells with higher growth rates must be developed.

Regarding GaAs solar cells, the EL2 trap, which is a common GaAs midgap complex defect involving arsenic antisites, is well known to deteriorate device performance among various deep-trap states in GaAs [14]. Schmieder reported that elevated growth rates were accompanied by an increased EL2 trap density, despite a constant input V/III ratio under standard MOVPE conditions [15]. For GaAs growth in HVPE using the arsine (AsH_3)–hydrogen chloride (HCl)–gallium (Ga)–hydrogen (H_2) system, the reaction process is known to change with the degree of AsH_3 thermal decomposition. AsH_3 easily decomposes to As_2 and As_4 species at a temperature above ~400 °C [16], which is considerably lower than the hot-wall reactor temperature of ~700 °C. When AsH_3 is thermally cracked in the reactor, the kinetic energy for the reaction of gallium chloride (GaCl) with As_4 is 200 kJ/mol, resulting in kinetically limited growth. Conversely, the kinetic energy can be considerably reduced to ~10 kJ/mol for the direct reaction of GaCl with AsH_3, resulting in mass transport-limited growth [17]. For the GaAs that are grown via HVPE under kinetically limited growth, Schulte reported that the growth with a low input V/III ratio could suppress the incorporation of arsenic into antisites owing to high GaCl coverage at the growth surface [18]. Moreover, Metaferia reported that an EL2 trap density of 1–3 $\times$ 10^{14} cm^{-3} across a wide range of growth rates (up to 309 µm/h) for HVPE-grown GaAs under mass transport-limited growth [19]. However, we also reported that cell performance deteriorated with increasing HVPE growth rate (up to 120 µm/h) under mass transport–limited growth, while the EL2 defect density has not been quantitatively evaluated [20]. Thus, the crystalline quality of GaAs seems to strongly depend on the growth conditions, such as the growth temperature, the partial pressure of each input material, and reaction kinetics. However, there have been few studies on the effect of the growth conditions on defect formation in HVPE-grown GaAs under mass transport-limited growth. This understanding is crucial for developing high-quality III-V solar cells with high throughput performance. In this study, the effect of growth conditions on HVPE-grown GaAs solar-cell properties was carefully evaluated in conjunction with defect analysis via deep-level transient spectroscopy (DLTS).

2. Materials and Methods

All samples were grown on 2″ GaAs(001) miscut 4° to the (111)B plane using a custom-built atmospheric-pressure HVPE (Taiyo Nippon Sanso, H260). The quartz reactor tube includes three chambers, i.e., two growth chambers and one preparation chamber. Details of the reactor design are shown in Figure 1. The reactor was heated using a six-zone clamshell resistance furnace. AsH_3, phosphine (PH_3), dimethylzinc (DMZn), hydrogen sulfide (H_2S), and disilane (Si_2H_6) were used as group-V and dopant sources, respectively. In a typical HVPE system, metal monochlorides such as GaCl and indium chloride (InCl),

are used as group–III precursors. The gaseous HCL in H_2 carrier gas was introduced at a flow rate of 1 standard liter per minute (SLM) into quartz boats that were filled with Ga and indium (In) metals to form GaCl and InCl. These two boats were heated at 700 °C to enhance the reaction efficiency. Conversely, growing Al-containing materials via HVPE is complicated because aluminum mono-chloride (AlCl) reacts with the reactor owing to its large equilibrium constant with respect to quartz [11]. In our HVPE system, $AlCl_3$ was generated at 500 °C instead of AlCl being generated in a different region to Ga and In boats. The temperature for the deposition region, where the susceptor was located, was maintained at 660 °C. The susceptor was shifted between the preparation chamber and each growth chamber within 1 s by a mechanical transfer arm.

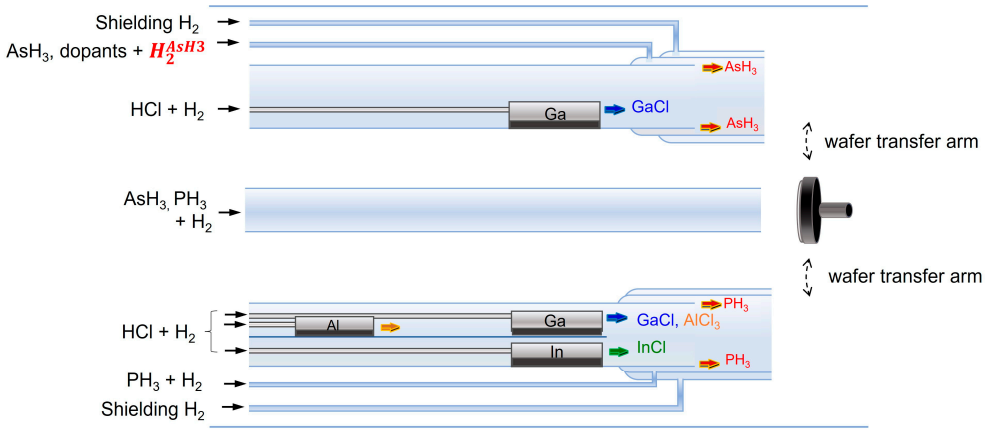

Figure 1. Schematic of the growth chambers in the custom-built hydride vapor phase epitaxy (HVPE) reactor. Dashed arrows indicate the direction of movement of the mechanical transfer arm between the preparation chamber and each growth chamber.

For device processing, AuGeNi/Au and Ti/Ag were formed for *n*- and *p*-type ohmic contacts using an electron beam evaporator. Metallization was performed at 350 °C for 2 min in ambient nitrogen. Front patterning and mesa isolation were conducted via standard photolithography.

The deep-trap states in GaAs were evaluated using a Semilab DLS-83D DLTS system. Cylindrical–structured p^+/n-GaAs diodes with a diameter of 1.0 mm were fabricated on *n*-type substrates (Figure 2a). This structure promotes evaluation of a low-doped *n*-GaAs base layer. All layers, except for the *n*-GaAs base layer, were grown with equivalent recipes. In the DLTS measurement system, DLTS signals are recorded using a lock-in amplifier synchronized to the corresponding measurement frequency defined by the inverse of the period width, T_w. The bias pulse width is denoted by T_p. To remove both the contribution of the capacitance transient during the bias pulse to the DLTS signal and the influence of the response time of the capacitance meter, as shown in [21], the capacitance transient was multiplied with a weighting function of zero in the time interval from the end of the bias pulse to $T_w/20$. The trap densities were calculated using the following equation to account for the lambda effect [22]:

$$N_t = \frac{2\varepsilon_0^2\varepsilon_r^2 A^2}{(W_r - \lambda)^2 - (W_p - \lambda)^2}\frac{\Delta C}{C_R^3}N_s \quad (1)$$

where N_t denotes the trap density, ε_0 denotes the vacuum permittivity, ε_r denotes the relative permittivity, A denotes the sample area, ΔC denotes the peak value of the DLTS signal, and N_s denotes the carrier density in the base layer. The variable W_r denotes the depletion width at the reverse-bias voltage, V_r, the variable W_p denotes the depletion width

during the bias pulse (pulse voltage V_p), and C_R denotes the capacitance value at V_r. The value of λ was calculated using following equation:

$$\lambda = \sqrt{\frac{2\varepsilon_0\varepsilon_r\left(E_f - E_t\right)}{q^2 N_s}} \quad (2)$$

where E_f denotes the quasi-Fermi level, E_t denotes the trap level, and q denotes the elementary charge.

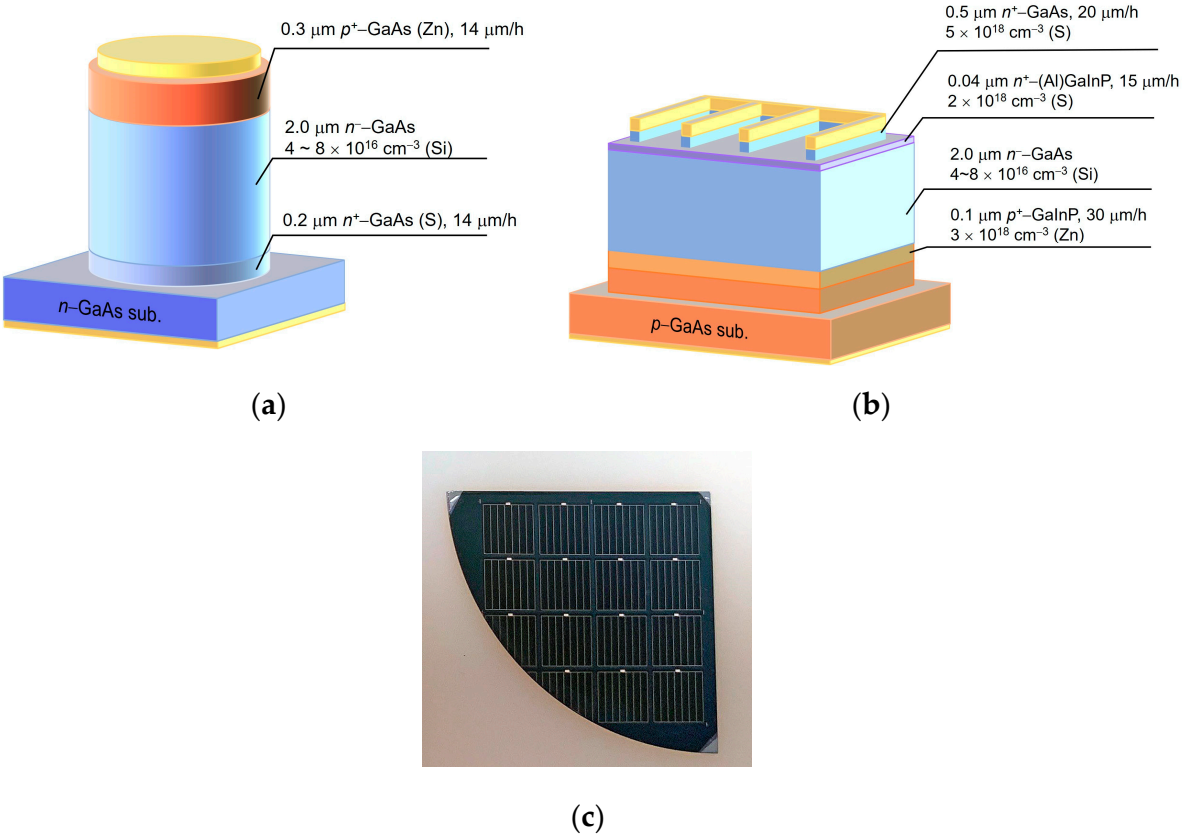

Figure 2. Schematic structure of (**a**) deep-level transient spectroscopy (DLTS) samples and (**b**) upright rear-heterojunction GaAs solar cells; (**c**) photograph of the solar cell device.

Upright rear-heterojunction GaAs solar cells were grown on *p*-type substrates (Figure 2b). All layers, except for the *n*-GaAs base layer, were grown with equivalent recipes. The growth rate was controlled from 49 up to 297 μm/h. For solar cell measurements, finger grids with 2.2% shadow loss were formed on the front side with an area of 0.25 cm^2 (Figure 2c). A ZnS (50-nm)/MgF_2 (100-nm) bilayer antireflection coating (ARC) was deposited on the front surface. Solar cells were characterized by measuring the external quantum efficiency (EQE) using chopped monochromated light with a constant photon flux of 1×10^{14} cm^{-2}. The current–voltage (*I*–*V*) characteristics were measured under air mass 1.5 global (AM1.5G) illumination at 100 mW/cm^2.

3. Results

3.1. GaAs Reaction Processes

As mentioned in Section 1, the degree of AsH_3 decomposition is crucial for the resulting GaAs reaction kinetics. In our HVPE system, GaAs is grown at the growth surface via following two reaction pathways:

$$GaCl + AsH_3 \rightarrow GaAs + HCl + H_2 \quad (3)$$

and

$$GaCl + \frac{1}{4}As_4 + \frac{1}{2}H_2 \rightarrow GaAs + HCl. \quad (4)$$

Here, the kinetic energy is ~10 kJ/mol for the direct reaction of GaCl with AsH_3 in Equation (3) resulting in mass transport-limited growth [17,21]. When AsH_3 is thermally cracked in the reactor, GaAs grows according to Equation (4). In this case, the kinetic energy is as large as 200 kJ/mol, resulting in kinetically limited growth.

To identify dominant reactions in our HVPE system, GaAs films were grown under various H_2 carrier gas (H_2^{AsH3}) flow rates (Figure 1). As H_2^{AsH3} can change the gas velocity, it is possible to control the AsH_3 spent time in the hot part of the reactor. The GaCl partial pressure (P_{GaCl}) was maintained at 8.8×10^{-4} atm. Further, the H_2^{AsH3} flow rate was varied from 3 to 10 slm, which was within the control range of our system. Considering the dimensions of the injector tube (with an inner diameter of 4 mm), the velocity considerably varied from 398 to 1326 cm/s when the H_2^{AsH3} flow rate was varied from 3 to 10 slm. Figure 3a shows the growth rate of GaAs as a function of the input V/III ratio under different H_2^{AsH3} flow rates. The growth rates were evaluated based on the thickness that was determined using a Nanometrics electrochemical capacitance–voltage (ECV) profiler and the known growth time. A detailed evaluation is described in Appendix A.

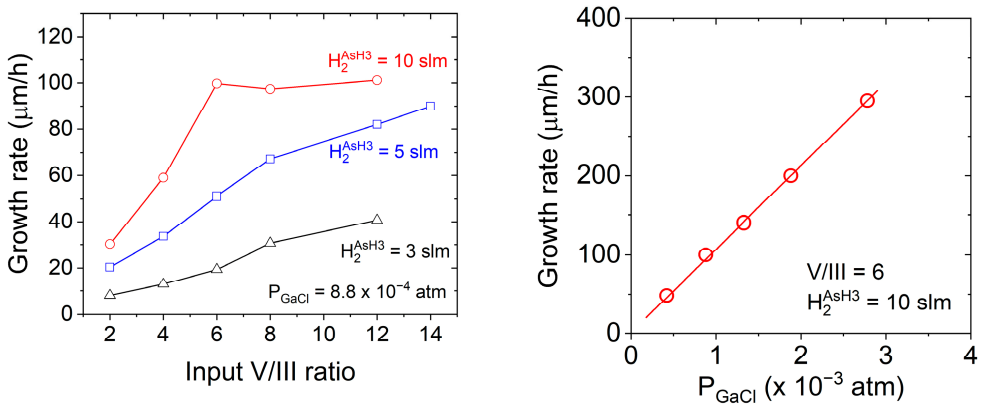

(**a**) (**b**)

Figure 3. GaAs growth rates under different H_2^{AsH3} flows as a function of (**a**) V/III ratio and (**b**) P_{GaCl}.

The growth rate increased with increasing the input V/III ratio for all cases, indicating the growth proceeded under AsH_3-poor conditions. Furthermore, a higher H_2^{AsH3} flow rate resulted in higher growth rates at the same V/III ratio, suggesting promotion of the direct reaction of GaAs with AsH_3. For the H_2^{AsH3} flow rate = 10 slm, the amount of GaCl and AsH_3 at the growth surface seemed to become unity at V/III = 6. Above V/III = 6, the growth rate was limited by the GaCl supply. Thus, H_2^{AsH3} flow rate was found to control the dominant reaction kinetics in GaAs growth in our HVPE system. Moreover, suppressing thermal decomposition of AsH_3 in the reactor is important to realize fast GaAs growth with low consumption of AsH_3. Figure 3b shows the growth rates as a function of P_{GaCl} for GaAs grown at V/III = 6 under a H_2^{AsH3} flow rate of 10 slm. The growth rate could be linearly increased up to 297 μm/h by increasing P_{GaCl} to 2.8×10^{-3} atm, indicating that GaAs growth proceeded under mass transport-limited growth.

3.2. DLTS Defect Analysis

We analyzed electron traps, which have a considerable impact on solar cell performance, in the *n*-GaAs films using the DLTS technique. In particular, it is crucial to understand the effect of the V/III ratio and reaction kinetics on the formation of electron

trap states because these traps are associated with intrinsic defects, which include antisites, interstitials, and vacancies of Ga and As atoms [14]. The inset of Figure 4a shows the DLTS spectra of samples whose *n*-GaAs layers were fabricated at a V/III ratio of 12 under different H_2^{AsH3} flow rates. The growth conditions were similar to those presented in Figure 3a. For DLTS measurements, we used $V_r = -2$ V, $V_p = 0$ V, $T_p = 1.0$ ms, and $T_w = 192$ ms. The activation energy (E_a) for the peak was determined from Arrhenius plots (not shown). A small peak at 180 K with $E_a = 0.4$ eV and a large peak at 355 K with $E_a = 0.8$ eV were observed for both spectra. These peaks are attributed to EL6 and EL2 defects, respectively. The EL2 trap is a complex defect involving As antisites, as mentioned in Section 1. The EL6 trap is also known as a complex defect involving arsenic interstitials [14]. In other words, arsenic-related intrinsic defects are dominantly generated under our HVPE growth conditions regardless of the growth kinetics. As the EL6 trap has a shallow trap energy with an order-of-magnitude lower peak intensity compared with that for the EL2 trap, the resulting solar cell performance is speculated to be primarily affected by EL2 traps. Figure 4a shows the EL2 trap density as a function of the input V/III ratio under two different H_2^{AsH3} flows rates. For both H_2^{AsH3} flow rates, the EL2 trap density increased with the input V/III ratio, suggesting that a high V/III ratio may promote the formation of EL2 defects. This is consistent with the observation that was reported by Schulte for GaAs grown via HVPE under kinetically limited growth [18]. The growth under a low input V/III ratio may suppress the incorporation of arsenic into anomalous sites owing to high GaCl coverage at the growth surface. At the same input V/III-ratio, the EL2 trap density for H_2^{AsH3} = 5 slm was slightly smaller than that for H_2^{AsH3} = 10 slm. This is because the growth at a low growth rate tends to promote surface migration of adatoms, leading to the incorporation of arsenic into normal sites. These results suggest that the EL2 trap density correlated with the input V/III ratio and the growth rate.

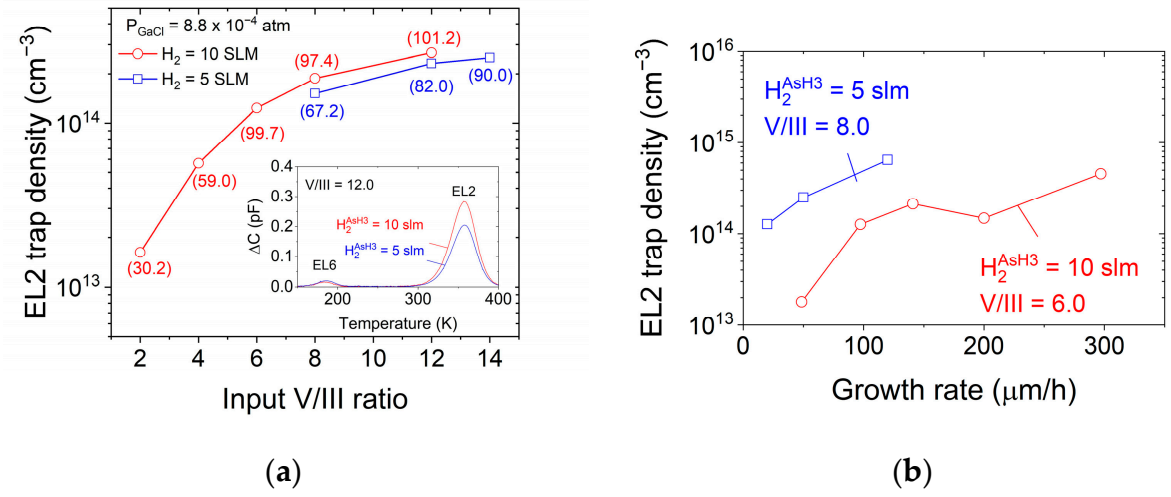

Figure 4. EL2 trap density in *n*-GaAs as a function of (**a**) input V/III ratio and (**b**) growth rate. The values in brackets indicate the growth rate for each condition. The inset of (**a**) shows the deep-level transient spectroscopy (DLTS) spectra of samples whose *n*-GaAs layers were fabricated at V/III = 12 under different H_2^{AsH3} flow rates of 5 and 10 slm.

Figure 4b compares the EL2 trap density as a function of the growth rate for *n*-GaAs grown under different conditions. The growth rate was controlled by the input material flow rate at a fixed input V/III ratio. The EL2 trap density tends to increase with increasing growth rate for both flow rates. As the surface migration length of adatoms decreases with increasing growth rates, the incorporation of arsenic into antisites may be promoted for faster growth. Notably, our obtained values were considerably smaller than that of 1.0×10^{15} cm^{-3} for MOVPE-grown GaAs at 56 μm/h [15]. As our HVPE growths were conducted using a lower input V/III ratio at a higher growth temperature than those in the

case of standard MOVPE growth conditions, the incorporation of arsenic into antisites could be suppressed owing to the superior surface migration length of adatoms. Furthermore, the EL2 trap densities for H_2^{AsH3} = 5 slm are larger than those for H_2^{AsH3} = 10 slm in the entire growth rate range owing to a large input V/III ratio. As mentioned in Section 3.1, this is because the thermal decomposition of AsH_3 in the reactor must be conpensated using a high AsH_3 flow rate for fast growth. However, the obtained values of 5.0×10^{14} cm^{-3} at 297 μm/h for H_2^{AsH3} = 10 slm are slightly larger than that of 3×10^{14} cm^{-3} that were reported by Metaferia [18]. The difference between these values may be explained based on the difference in the degree of AsH_3 thermal decomposition in the HVPE reactor. Thus, further suppressing the AsH_3 thermal decomposition in the HVPE reactor is desirable to achieve high-quality GaAs with reduced EL2 trap density. Equipment improvements based on these results are currently underway.

3.3. GaAs Solar Cell Performance

Figure 5 shows the short-circuit current density (J_{SC}), open-circuit voltage (V_{OC}), fill factor (*FF*), and η for GaAs solar cells grown with GaInP window layers at various growth rates. The ARC was not used for these cells. A total of eight cells that were fabricated on identical wafers were measured for each growth rate. The growth conditions for the *n*-GaAs base layer were similar to the samples for which H_2^{AsH3} = 10 slm in Figure 4b. Although the slight deviation of cell characteristics between growth rates is considered to be caused by the difference in the base-layer thickness and carrier concentration, almost no considerable deterioration of cell characteristics is observed up to a growth rate of 297 μm/h. Notably, all the cells exhibited a bandgap-V_{OC} deficit (W_{OC}) of <0.40 V, which is a standard benchmark for high-quality material solar cells [23]. However, the V_{OC} for a growth rate of 297 μm/h was the smallest among all values. To evaluate the effect of EL2 traps on cell performance, the nonradiative lifetime (τ_{nr}) was calculated using following equations:

$$\tau_{nr} = \frac{1}{\sigma v_{th} N_t} \tag{5}$$

and

$$v_{th} = \sqrt{\frac{3k_B T}{m^*}} \tag{6}$$

where σ denotes the capture cross section, N_t denotes the trap density, k_B denotes the Boltzmann constant, T denotes the temperature, and m^* denotes the effective mass, respectively. Using 3.1×10^{-16} cm^2 for σ reported in [18], the τ_{nr} was calculated to be 3969.6, 546.0, 335.4, 158.7, and 152.7 ns for the cells that were grown at 49, 97, 141, 200, and 297 μm/h, respectively. τ_{nr} approached closer to a radiative lifetime of ~125 ns with increasing growth rate. Therefore, a short τ_{nr} is considered to be one of the factors for the lowered V_{OC} for cell growth at 297 μm/h. Another factor is that the in-plane uniformity may be degraded due to fast growth under excessively high H_2^{AsH3} considering that the deviation of the 297-μm/h cell is larger than the other cells. Therefore, it is also necessary to improve the in-plane uniformity of the input material at the growth surface for maintaining cell characteristics at an ultrafast growth rate.

Finally, GaAs solar cells that were grown with different window layers at a growth rate of 200 μm/h are compared in Figure 6. Lattice-matched GaInP or $Al_{0.25}Ga_{0.25}In_{0.5}P$ were used for the window layer. The detailed growth conditions for the AlGaInP are provided in [11,24]. By replacing the window material from GaInP to AlGaInP, the EQE response in the short wavelength region, below 650 nm, was considerably increased owing to the widening of the window-layer bandgap. This led to the improved J_{SC}, from 26.83 to 29.10 mA/cm^2. However, there was no clear difference in the V_{OC} and *FF* because these parameters are mainly determined by *p*/*n* junction properties. The smaller *FF* compared with that reported in [19] possibly due to nonoptimized finger grids. The obtained η of 24.0% is comparable with the reported values for high-speed MOVPE [15,25,26] and HVPE [13,19]. The solar cell performance can be further improved by applying a wide

bandgap AlInP material to the window layer [13] or an inverted thin-film structure that can enhance light trapping [27].

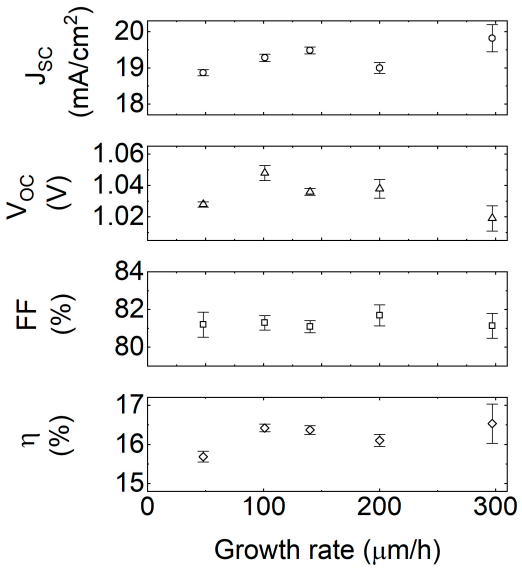

Figure 5. Cell parameters for GaAs solar cells grown at various growth rates with an input V/III ratio of 6 under a H_2 carrier gas (H_2^{AsH3}) flow rate of 10 slm.

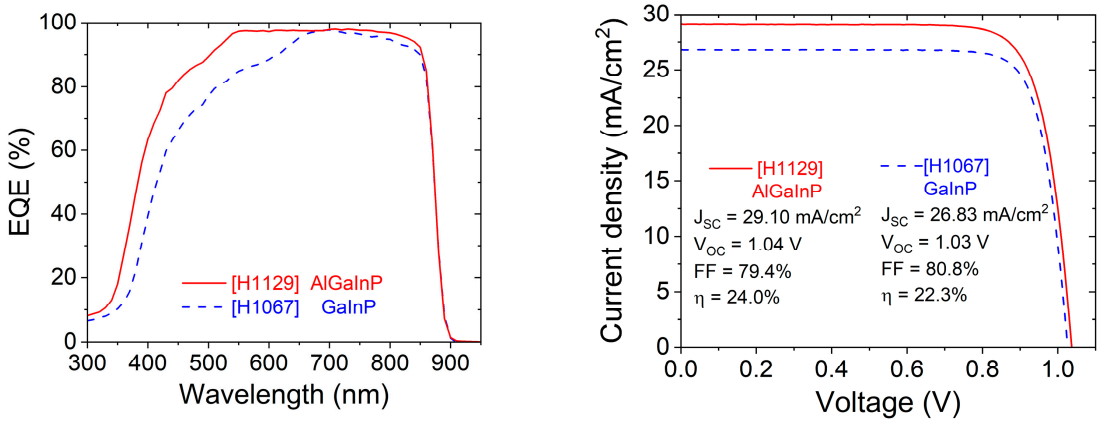

(**a**) (**b**)

Figure 6. (**a**) External quantum efficiency (EQE) and (**b**) illuminated *I*–*V* curve spectra for GaAs solar cells grown with different window layers at a growth rate of 200 μm/h.

4. Conclusions

We carefully investigated the effect of atmospheric-pressure triple-chamber HVPE high-speed growth conditions on the properties of GaAs solar cells. Suppressing the AsH_3 thermal decomposition of the reactor was found to be effective at achieve fast growth usinging a low input V/III ratio. The DLTS results revealed that suppressing the thermal decomposition of AsH_3 in the hot-wall reactor was effective for achieving high-speed growth with a lower V/III-input ratio and reducing the EL2 trap density at a given growth rate. This was probably because the low input V/III ratio may have suppressed the incorporation of arsenic into anomalous sites owing to high GaCl coverage at the growth surface. Solar cell characterization showed that the performance of GaAs solar cells grown under reduced AsH_3 thermal cracking exhibited almost no considerable deterioration up to a growth rate of 297 μm/h. Consequently, a conversion efficiency of 24.0% was obtained for GaAs solar cells grown at 200 μm/h. Our future research will focus on the fast growth

of GaInP solar cells and the development of ultrafast GaInP/GaAs dual-junction solar cells. This study represents an important step toward the development of low-cost and highly efficient III-V multijunction devices.

Author Contributions: Conceptualization, R.O. and Y.S.; Data curation, R.O. and A.O.; Formal analysis, A.O.; Funding acquisition, S.K. and T.S.; Investigation, R.O. and A.O.; Methodology, R.O. and A.O.; Project administration, S.K. and T.S.; Resources, A.U., S.K., M.I. and T.S.; Supervision, K.M., A.U., S.K., M.I. and T.S.; Validation, R.O. and A.O.; Visualization, R.O.; Writing–original draft, R.O.; Writing–review and editing, A.O., Y.S., K.M., A.U., S.K., M.I. and T.S. All authors have read and agreed to the published version of the manuscript.

Funding: This research was funded by the New Energy and Industrial Technology Development Organization (NEDO), grant number JPNP20015.

Data Availability Statement: Not applicable.

Acknowledgments: It is my pleasure to acknowledge Hideo Kumagai for sample growth, Shunichi Kato and Kumi Hayashi for sample processing, and Jiro Nishinaga for valuable discussion on DLTS measurements.

Conflicts of Interest: The authors declare no conflict of interest.

Appendix A

The growth rates for all layers that were described in this study were based on separate electrochemical capacitance–voltage (ECV) measurements. Depth profiling was achieved via electrolytical etching between CV measurements. The strengths of this technique are simple sample preparation, direct correspondence of the measured magnitudes to the active carrier concentration and depth, and unlimited profiling depth [28]. Figure A1 shows the depth profile for the five growth steps of Si-doped GaAs films that were grown under a H_2^{AsH3} flow rate of 10 slm using different input V/III ratios. We employed ethylenediamine tetraacetic acid disodium as an electrolyte, corresponding to the result in Figure 3a. Based on Figure A1, the thickness of each step was determined to be 0.251, 0.492, 0.831, 0.812, and 0.843 µm for *n*-GaAs grown using input V/III ratios of 2, 4, 6, 8, and 12, respectively. By accounting for the growth time for each layer (30 s), the growth rates were calculated to be 30.2, 59.0, 99.7, 97.4, and 101.2 µm/h.

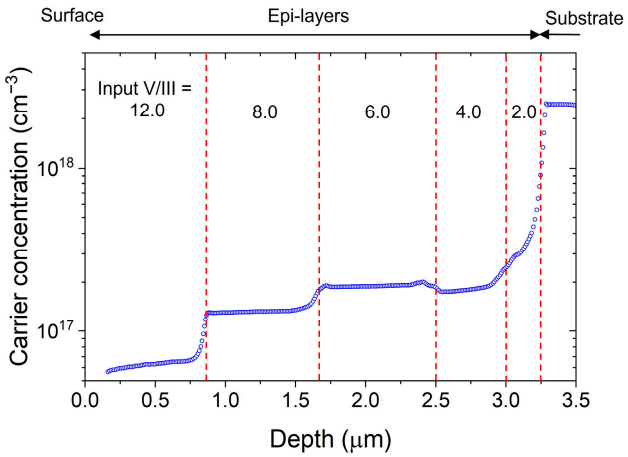

Figure A1. Active electron concentration as a function of depth for five growth steps of Si-doped GaAs films grown under an H_2 carrier gas (H_2^{AsH3}) flow rate of 10 slm with different input V/III ratios measured using an electrochemical capacitance–voltage (ECV) profiler. The growth time for each layer was 30 s. Red dotted lines denote interfaces between Si-doped GaAs layers grown at different input V/III ratio.

References

1. Masuda, T.; Araki, K.; Okumura, K.; Urabe, S.; Kudo, Y.; Kimura, K.; Nakado, T.; Sato, A.; Yamaguchi, M. Static concentrator photovoltaics for automotive applications. *Sol. Energy* **2017**, *146*, 523–531. [CrossRef]
2. Yablonovitch, E.; Gmitter, T.; Harbison, J.P.; Bhat, R. Extreme selectivity in the lift-off of epitaxial GaAs films. *Appl. Phys. Lett.* **1987**, *51*, 2222–2224. [CrossRef]
3. Shahrjerdi, D.; Bedell, S.W.; Bayram, C.; Lubguban, C.C.; Fogel, K.; Lauro, P.; Ott, J.A.; Hopstaken, M.; Gayness, M.; Sadana, D. Ultralight high-Efficiency flexible InGaP/(In)GaAs tandem solar cells on plastic. *Adv. Energy Mater.* **2013**, *3*, 566–571. [CrossRef]
4. Green, M.A.; Dunlop, E.D.; Hohl-Ebinger, J.; Yoshita, M.; Kopidakis, N.; Bothe, K.; Hinken, H.; Rauer, M.; Hao, X. Solar cell efficiency tables (Version 60). *Prog. Photovolt. Res. Appl.* **2022**, *30*, 687–701. [CrossRef]
5. Müller, R.; Schygulla, P.; Lackner, D.; Höhn, O.; Hauser, H.; Richter, A.; Fell, A.; Bläsi, B.; Predan, P.; Benick, J.; et al. Silicon-based monolithic triple-junction solar cells with conversion efficiency >34%. In Proceedings of the 37th European Photovoltaic Solar Energy Conference and Exhibition, Lisbon, Portugal, 7–11 September 2020; pp. 574–578.
6. Essig, S.; Allebé, C.; Remo, T.; Geisz, J.F.; Steiner, M.A.; Horowitz, K.; Barraud, L.; Scott Ward, J.; Schnabel, M.; Descoeudres, A.; et al. Raising the one-sun conversion efficiency of III–V/Si solar cells to 32.8% for two junctions and 35.9% for three junctions. *Nat. Energy* **2017**, *2*, 17144. [CrossRef]
7. Makita, K.; Kamikawa, Y.; Koida, T.; Mizuno, H.; Oshima, R.; Shoji, Y.; Ishizuka, S.; Takamoto, T.; Sugaya, T. Mechanical stacked GaAs//$CuIn_{1-y}Ga_ySe_2$ three-junction solar cells with 30% efficiency via an improved bonding interface and area current-matching technique. *Prog. Photovolt. Res. Appl.* **2023**, *31*, 71–84. [CrossRef]
8. McClure, E.L.; Schulte, K.L.; Simon, J.; Metaferia, W.; Ptak, A.J. GaAs growth rates of 528 µm/h using dynamic-hydride vapor phase epitaxy with a nitrogen carrier gas. *Appl. Phys. Lett.* **2020**, *116*, 182102. [CrossRef]
9. Grüter, K.; Deschler, M.; Jürgensen, H.; Beccard, R.; Balk, P. Deposition of high-quality GaAs films at fast rates in the LP-CVD system. *J. Cryst. Growth* **1989**, *94*, 607–612. [CrossRef]
10. Oshima, R.; Makita, K.; Ubukata, A.; Sugaya, T. Improvement of heterointerface properties of GaAs solar cells grown with InGaP layers by hydride vapor-phase epitaxy. *IEEE J. Photovolt.* **2019**, *9*, 154–159. [CrossRef]
11. Shoji, Y.; Oshima, R.; Makita, K.; Ubukata, A.; Sugaya, T. InGaP/GaAs dual-junction solar cells with AlInGaP passivation layer grown by hydride vapor phase epitaxy. *Prog. Photovolt. Res. Appl.* **2021**, *29*, 1285–1293. [CrossRef]
12. Shoji, Y.; Oshima, R.; Makita, K.; Ubukata, A.; Sugaya, T. 28.3% efficient III–V tandem solar cells fabricated using a triple-chamber hydride vapor phase epitaxy system. *Sol. RRL* **2022**, *6*, 2100948. [CrossRef]
13. Boyer, J.T.; Schulte, K.L.; Young, M.R.; Ptak, A.J.; Simon, J. AlInP-passivated III–V solar cells grown by dynamic hydride vapor-phase epitaxy. *Prog. Photovolt. Res. Appl.* **2022**, *31*, 230–236. [CrossRef]
14. Reddy, C.V.; Fung, S.; Beling, C.D. Nature of the bulk defects in GaAs through high-temperature quenching studies. *Phys. Rev. B* **1996**, *54*, 11290–11297. [CrossRef]
15. Schmieder, K.J.; Armour, E.A.; Lumb, M.P.; Yakes, M.K.; Pulwin, Z.; Frantz, J.; Walters, R.J. Effect of growth temperature on GaAs solar cells at high MOCVD growth rates. *IEEE J. Photovolt.* **2017**, *7*, 340–346. [CrossRef]
16. Ban, V.S. Mass spectrometric and thermodynamics studies of the CVD of some III–V compounds. *J. Cryst. Growth* **1972**, *17*, 19–30. [CrossRef]
17. Schulte, K.L.; Braun, A.; Simon, J.; Ptak, A.J. High growth rate hydride vapor phase epitaxy at low temperature through use of uncracked hydrides. *J. Appl. Phys.* **2018**, *112*, 042101. [CrossRef]
18. Schulte, K.L.; Kuech, T.F. A model for arsenic anti-site incorporation in GaAs grown by hydride vapor phase epitaxy. *J. Appl. Phys.* **2014**, *116*, 243504. [CrossRef]
19. Metaferia, W.; Schulte, K.L.; Simon, J.; Johnston, S.; Ptak, A.J. Gallium arsenide solar cells grown at rates exceeding 300 µm h^{-1} by hydride vapor phase epitaxy. *Nat. Commun.* **2019**, *10*, 3361. [CrossRef]
20. Oshima, R.; Shoji, Y.; Makita, K.; Ubukata, A.; Sugaya, T. Evaluation of GaAs solar cells grown under different conditions via hydride vapor phase epitaxy. *J. Cryst. Growth* **2020**, *537*, 125600. [CrossRef]
21. Tokuda, Y.; Shimizu, N.; Usami, A. Studies of neutron-produced defects in silicon by deep-level transient spectroscopy. *Jpn. J. Appl. Phys.* **1979**, *18*, 309–315. [CrossRef]
22. Zohta, Y.; Watanabe, M.O. On the determination of the spatial distribution of deep centers in semiconducting thin films from capacitance transient spectroscopy. *J. Appl. Phys.* **1982**, *53*, 1809–1811. [CrossRef]
23. King, R.R.; Bhusari, D.; Boca, A.; Larrabee, D.; Liu, X.Q.; Hong, W.; Fetzer, C.M.; Law, D.C.; Karam, N.H. Band gap-voltage offset and energy production in next-generation multijunction solar cells. *Prog. Photovolt. Res. Appl.* **2011**, *19*, 797–812. [CrossRef]
24. Shoji, Y.; Oshima, R.; Makita, K.; Ubukata, A.; Sugaya, T. III-V solar cells with AlInGaP window layer grown by low-cost hydride vapor phase epitaxy. In Proceedings of the 31st International Photovoltaics Science and Engineering Conference, Online, 13–15 December 2021.
25. Sodabanlu, H.; Ubukata, A.; Watanabe, K.; Koseki, S.; Matsumoto, K.; Sugaya, T.; Nakano, Y.; Sugiyama, M. 24.5% efficient GaAs p-on-n solar cells with 120 µm h^{-1} MOVPE growth. *J. Phys. D Appl. Phys.* **2019**, *52*, 105501. [CrossRef]
26. Lang, R.; Schön, J.; Dimroth, F.; Lackner, D. Optimization of GaAs solar cell performance and growth efficiency at MOVPE growth rates of 100 µm/h. *IEEE J. Photovolt.* **2018**, *8*, 1596–1600. [CrossRef]

27. Geisz, J.F.; Steiner, M.A.; García, I.; Kurtz, S.R.; Friedman, D.J. Enhanced external radiative efficiency for 20.8% efficient single-junction GaInP solar cells. *Appl. Phys. Lett.* **2013**, *103*, 041118. [CrossRef]
28. Peiner, E.; Schlachetzki, A.; Krüger, D. Doping profile analysis in Si by electrochemical capacitance-voltage measurements. *J. Electrochem. Soc.* **1995**, *142*, 576–580. [CrossRef]